Super-luminous supernovae at redshifts of 2.05 and 3.90

Jeff Cooke[1], Mark Sullivan[2], Avishay Gal-Yam[3], Elizabeth J. Barton[4], Raymond G. Carlberg[5], Emma V. Ryan-Weber[1], Chuck Horst[6], Yuuki Omori[7] & C. Gonzalo Díaz[1]

[1]*Centre for Astrophysics and Supercomputing, Swinburne University of Technology, PO Box 218, H30, Hawthorn, VIC, 3122, Australia*
[2]*Department of Physics, University of Oxford, Denys Wilkinson Building, Keble Road, Oxford OX1 3RH, UK*
[3]*Benoziyo Center for Astrophysics, Weizmann Institute of Science, 76100 Rehovot, Israel*
[4]*Center for Cosmology, Department of Physics and Astronomy, University of California, Irvine, CA 92697, USA*
[5]*Department of Astronomy and Astrophysics, University of Toronto, Toronto, ON M5S 3H4, Canada*
[6]*Department of Astronomy, San Diego State University, San Diego, CA, 92182, USA*
[7]*Department of Physics, McGill University, 3600 rue University, Montreal, QC H2A 2T8, Canada*

A rare class of 'super-luminous' supernovae that are about ten or more times more luminous at their peaks than other types of luminous supernovae has recently been found at low to intermediate redshifts.[1,2] A small subset of these events have luminosities that evolve slowly and result in radiated energies of around 10^{51} ergs or more. Therefore, they are likely examples of 'pair-instability' or 'pulsational pair-instability' supernovae with estimated progenitor masses of 100 - 250 times that of the Sun.[3–5] These events are exceedingly rare at low redshift, but are expected to be more common at high redshift because the mass distribution of the earliest stars was probably skewed to high values.[6,7] Here we report the detection of two super-luminous supernovae, at redshifts of 2.05 and 3.90, that have slowly evolving light curves. We estimate the rate of events at redshifts of 2 and 4 to be approximately ten times higher than the rate at low redshift. The extreme luminosities of super-luminous supernovae extend the redshift limit for supernova detection using present technology, previously 2.36 (ref.8), and provide a way of investigating the deaths of the first generation of stars to form after the Big Bang.

We search for high redshift super-luminous supernovae (SLSNe) by modifying our image stacking and analysis technique[9] to their expected light-curve evolution and high luminosities as recently determined from theory and low-redshift observations. Supernovae SN 2213-1745 and SN 1000+0216 were discovered when applying our modified technique to the Canada-France-Hawaii Telescope Legacy Survey Deep Fields. The archival survey data provide deep, consistent photometry of the host galaxies over ∼6 month seasons from 2003 to 2008 and enable clean extraction of the supernova restframe far-ultraviolet light. Follow-up late-time spectroscopy of the supernovae and their host galaxies was obtained using the 10-m Keck I telescope 5.2 and 3.8 yr (∼626 and ∼286 d, restframe) after first detection for SN 2213-1745 and SN 1000+0216, respectively. The deep Keck data reveal redshifts of $z = 2.0458$ for SN 2213-1745 and $z = 3.8993$ for SN 1000+0216. Details of the supernovae and their host galaxies are listed in Table 1.

SN 2213-1745 is detected in the 2005 and 2006 seasonal (June - November) stacked images for the field D4, and SN 1000+0216 is detected in the 2006-2007 and 2007-2008 seasonal (November - June) stacked images for field D2 (Figure 1). Neither supernovae is

detected in the previous two seasons down to the stacked image detection limits of m $\sim$ 26.5 mag (Supplementary Information, section A). The nightly images that comprise the seasonal stacks first show the supernovae at the onset of the observing seasons. The lack of detection in previous seasons implies that the initial outbursts occurred between November 2004 and June 2005 for SN 2213-1745 and between June and November 2006 for SN 1000+0216. Both supernovae evolve slowly and reach high peak luminosities of $\sim$0.5 - 1$\times$10^{44} erg s^{-1}, uncorrected for host galaxy extinction. The peak luminosities correspond to far-ultraviolet absolute AB magnitudes[10,11] of M$_{peak}$ $\sim$ -21 mag and thereby rule out all normal supernova subtypes. SLSNe are the only supernova type that can generate similar peak magnitudes and light curve evolution (Figure 2).

Although active galactic nuclei (AGN), powered by the erratic accretion of material onto supermassive black holes at the centres of galaxies, can produce similar energies, both host galaxies exhibit a single supernova-like outburst, present no activity during the previous two years and have colours that are inconsistent with high redshift AGN, including the eight spectroscopic AGN in our sample. Moreover, the SN 2213-1745 host spectrum does not show signs of AGN activity (Figure 3), and although the SN 1000+0216 host spectrum shows narrow Lyα emission, common to high redshift galaxies, no other AGN-associated features are seen. In contrast, the images reveal zero, or very small, separations (projected in the plane of the sky) from their host galaxy centroids (Supplementary Information, section A). We note that our technique is limited to detecting supernovae within the small extent of the high-redshift host galaxies that produces far-ultraviolet flux, and that far-ultraviolet light directly traces regions of high star formation and does not necessarily provide accurate galaxy centroids. Finally, although the ultraviolet-optical afterglows of long-duration gamma ray bursts can achieve luminosities equivalent to, or greater than, the observed events, the bursts typically reach their peak luminosities within a day and quickly decay,[12] usually following a power law of the form t$^\beta$, with β $\sim$ -1. This behaviour is inconsistent with the observed slow rise and slow decay of the events discussed here.

Recently, SLSNe have been classified into groups on the basis of their photometric and spectroscopic properties[2]. Those in group SLSN-I show no evidence of hydrogen in their spectra, whereas those in group SLSN-II are rich in hydrogen and include a subset showing signs of interaction with circumstellar material. Finally, those in group SLSN-R have light curves that evolve slowly, powered by the radiative decay of ^{56}Ni. SLSN-R events are suspected to be pair-instability supernovae; the deaths of stars with initial masses between 140 - 260 solar masses[3–5]. The physics of the pair-instability process has been understood for many years, but the extreme rarity of SLSN-R ($\sim$10 times less frequent than SLSN-I or SLSN-II) has resulted in only one believable recorded event, SN 2007bi[13], which is well studied up to late times, with a few candidates being followed by ongoing low-redshift surveys.

In Figure 2, we compare the photometric evolution of the high-redshift supernovae with lower-redshift SLSN data at similar wavelengths.[14–18] All SLSNe, except for SLSN-R SN 2007bi which is believed to be powered by $\sim$4 - 7 solar masses of ^{56}Ni, fade significantly quicker than the two high-redshift events. As far as can be determined from the photometry, the evolution of SN 2213-1745 is consistent with SN 2007bi and, as a result, provides the first far-ultraviolet data for an SLSN-R. The close agreement suggests that SN 2213-1745 may be powered by the radiative decay of a similar amount of synthesised ^{56}Ni, and, along with an integrated radiated luminosity of $\sim$10^{51} erg, implies a progenitor with an estimated initial mass of $\sim$250 solar masses. We note that although SN 2213-1745 is shown to follow closely the luminosity evo-

lution of a radiation-hydrodynamics SLSN-R simulation[19] for a progenitor star of similar mass, the observed flux is higher and bluer than the model expectations (Supplementary Information, section C).

SN 1000+0216 was observed over a shorter time period than was SN 2213-1745, as a result of time dilation. The range of the light curve sampled suggests a slower rise time than SN 2213-1745 but appears to follow a similar fade rate from peak luminosity to $\sim$50 d later, restframe, if we assume that the peak occurred during the gap in coverage between the two detection seasons. The peak far-ultraviolet magnitude of SN 1000+0216 may exceed that possible for a pair-instability supernova. As a result, SN 1000+0216 may be an example of a pulsational pair-instability supernova[5] or a SLSN-II similar to the low redshift SN 2006gy[20,21], which experience enhanced luminosity as a result of interaction with previously expelled circumstellar material (Supplementary Information, sections D & F). The high luminosity of SN 1000+0216 classifies it as a SLSN but, because of its limited photometric coverage and low signal-to-noise host spectrum, its subclassification remains uncertain.

Our programme searches for $z \gtrsim 2$ supernovae by monitoring the well-studied population of Lyman break galaxies[22–24] over several well-defined volumes. Because Lyman break galaxies comprise the bulk of galaxies at high redshift, where star formation rates are higher, normal populations of short-lived, massive stars are more common at $z \gtrsim 2$ than locally. From the specifics of our survey, the two SLSN detections imply a rough volumetric high-redshift rate of a few $\times$ 10^{-7} h_{71}^3 Mpc^{-3} yr^{-1} at $z = 2.2 \pm 0.3$ and $z = 4.1 \pm 0.3$ (mean $\pm 1\sigma$)(Supplementary Information, section B). After correcting for the increase in the cosmic star formation rate from low to high redshift, the SLSN rate remains $\sim$10 times higher than that estimated at low-redshift[1], but we caution that our rate estimate is poorly constrained because it is derived from only two events. The far-ultraviolet photometry confirms that the two supernovae are strong sources of escaping high-energy photons. However, far-ultraviolet light is highly susceptible to metal-line absorption and local and global dust extinction that may have a greater effect on other high redshift SLSNe and cause them to fall below our detection threshold. As a result, our estimated rate is a lower limit and implies that the discrepancy between low and high redshift may be even greater.

The detection of SLSNe at $z > 2$ presents the possibility of finding the explosions of Population III stars, the first stars to form after the Big Bang. Population III stars are predicted to exist a redshifts as low as $z \sim 2$ (refs 25-28) and have mass distributions skewed towards high masses[6,7]. On the basis of our late-time spectroscopy, the supernovae presented here are unlikely to be from the first generation stars (Supplementary Information, section E). Deep spectroscopy of future supernovae obtained near maximum brightness, and their use as sightline probes, offers a means to help distinguish which events formed in regions with essentially no enrichment in elements heavier than helium, and thus likely had Population III progenitors.

REFERENCES

1. Quimby, R. M. *et al.* Hydrogen-poor superluminous stellar explosions *Nature* **474**, 487–489 (2011).

2. Gal-Yam, A. *et al.* Super-luminous Supernovae *Science* **337**, 927–932 (2012).

3. Rakavy, G. & Shaviv, G. Instabilities in Highly Evolved Stellar Models *Astrophys. J.* **148**, 803–816 (1967).

4. Barkat, Z., Rakavy, G. & Sack, N. Dynamics of Supernova Explosion Resulting from Pair Formation *Phys. Rev. Lett.* **18**, 379–381 (1967).

5. Heger, A. & Woosley, S. E. The Nucleosynthetic Signature of Population III *Astrophys. J.* **567**, 532–543 (2002).

6. Larson R. B. Early star formation and the evolution of the stellar initial mass function in galaxies *Mon. Not. R. Astron. Soc.* **301**, 569–581 (1998).

7. Bromm, V., Coppi, P. S. & Larson, R. B. Forming the First Stars in the Universe: The Fragmentation of Primordial Gas *Astrophys. J. Lett.* **527**, L5-L8 (1999).

8. Cooke J. *et al.* Type IIn supernovae at redshift z˜2 from archival data *Nature* **460**, 237–239 (2009).

9. Cooke J. Detecting $z > 2$ Type IIn Supernovae *Astrophys. J.* **677**, 137–145 (2008).

10. Oke J. B. Absolute Spectral Energy Distributions for White Dwarfs *Astrophys. J. Suppl. Ser.* **27**, 21–35 (1974).

11. Fukugita, M. *et al.* The Sloan Digital Sky Survey Photometric System *Astron. J.* **111**, 1748–1756 (1996).

12. Kann, D. A. *et al.* The Afterglows of Swift-era Gamma-Ray Bursts. II. Type I GRB versus Type II GRB Optical Afterglows *Astrophys. J.* **734**, 96–150 (2011).

13. Gal-Yam, A. *et al.* Supernova 2007bi as a pair-instability explosion *Nature* **462**, 624–627 (2009).

14. Gezari, S. *et al.* Discovery of the Ultra-Bright Type II-L Supernova 2008es *Astrophys. J.* **690**, 1313–1321 (2009).

15. Barbary, K. *et al.* Discovery of an Unusual Optical Transient with the Hubble Space Telescope *Astrophys. J.* **690**, 1358–1362 (2009).

16. Pastorello, A. *et al.* Ultra-Bright Optical Transients Are Linked With Type Ic Supernovae *Astrophys. J. Lett.* **724**, 16–21 (2010)

17. Young, D. R. *et al.* Two type Ic supernovae in low-metallicity, dwarf galaxies: diversity of explosions *Astron. Astrophys.* **512**, A70 (2010)

18. Chomiuk, L. *et al.* PAN-STARRS1 Discovery of two ultra-luminous supernovae at $z \sim 0.9$ *Astrophys. J.* **743**, 114 (2011).

19. Kasen, D., Woosley, S. E. & Heger, A. Pair Instability Supernovae: Light Curves, Spectra, and Shock Breakout *Astrophys. J.* **734**, 102 (2011).

20. Smith, N. *et al.* SN 2006gy: Discovery of the most luminous supernova ever recorded, powered by the death of an extremely massive star like η Carinae *Astrophys. J.* **666**, 1116–1128 (2007).

21. Smith, N. *et al.* Spectral Evolution of the Extraordinary Type IIn Supernova 2006gy *Astrophys. J.* **709**, 856–883 (2010).

22. Steidel, C. C. *et al.* Lyman-Break Galaxies at $z \gtrsim 4$ and the Evolution of the Ultraviolet Luminosity Density at High Redshift *Astrophys. J.* **519**, 1–17 (1999).

23. Steidel, C. C. *et al.* Lyman Break Galaxies at Redshift $z \sim 3$: Survey Description and Full Data Set *Astrophys. J.* **592**, 728–754 (2003).

24. Steidel, C. C. *et al.* A Survey of Star-Forming Galaxies in the $1.4 < z < 2.5$ Redshift Desert: Overview *Astrophys. J.* **604**, 534–550 (2004).

25. Scannapieco, E. *et al.* The Detectability of Pair-Production Supernovae at $z < 6$ *Astrophys. J.* **633**, 1031–1041 (2005).

26. Tornatore, L., Ferrara, A. & Schneider, R. Population III stars: hidden or disappeared? *Mon. Not. R. Astron. Soc.* **382**, 945–950 (2007).

27. Trenti, M., Stiavelli, M. & Michael Shull, J. Metal-free Gas Supply at the Edge of Reionization: Late-epoch Population III Star Formation *Astrophys. J.* **700**, 1672–1679 (2009).

28. Fumagalli, M., O'Meara, J. M. & Prochaska, J. X. Detection of Pristine Gas Two Billion Years After the Big Bang *Science* **334**, 1245–1249 (2011).

29. Schlegel, D. J., Finkbeiner, D. P. & Davis, M. Maps of Dust Infrared Emission for Use in Estimation of Reddening and Cosmic Microwave Background Radiation Foregrounds *Astrophys. J.* **500**, 525–553 (1998).

Supernova	R.A. (J2000)	Dec. (J2000)	Host M_{FUV}	SN peak M_{FUV}	Detection dates	Redshift (z)
SN 2213-1745	22 13 39.970	-17 45 24.486	-21.38$\pm$0.03	-21.2$\pm$0.2	Jun 2005 - Nov 2006	2.0458$\pm$0.0005
SN 1000+0216	10 00 05.862	+02 16 23.621	-21.20$\pm$0.04	-21.6$\pm$0.2	Nov 2006 - Jun 2008	3.8993$\pm$0.0074

Table 1: Supernova and host galaxy details. The far-ultraviolet absolute magnitudes, M_{FUV} are derived using the conventional relationship $M_{FUV} = m_{AB} - 5 \cdot \log_{10}(D_L(z)/10pc) + 2.5 \cdot \log_{10}(1+z)$, where m_{AB} is the observed redshifted far-ultraviolet AB magnitude[10,11] and D_L is the luminosity distance, adopting a standard $H_0 = 71$, $\Omega_\Lambda = 0.73$, $\Omega_M = 0.27$ cosmology. The supernova absolute magnitudes are corrected for extinction by the Milky Way Galaxy[29] (0.04 - 0.11 mag) but not corrected for supernova host galaxy extinction.
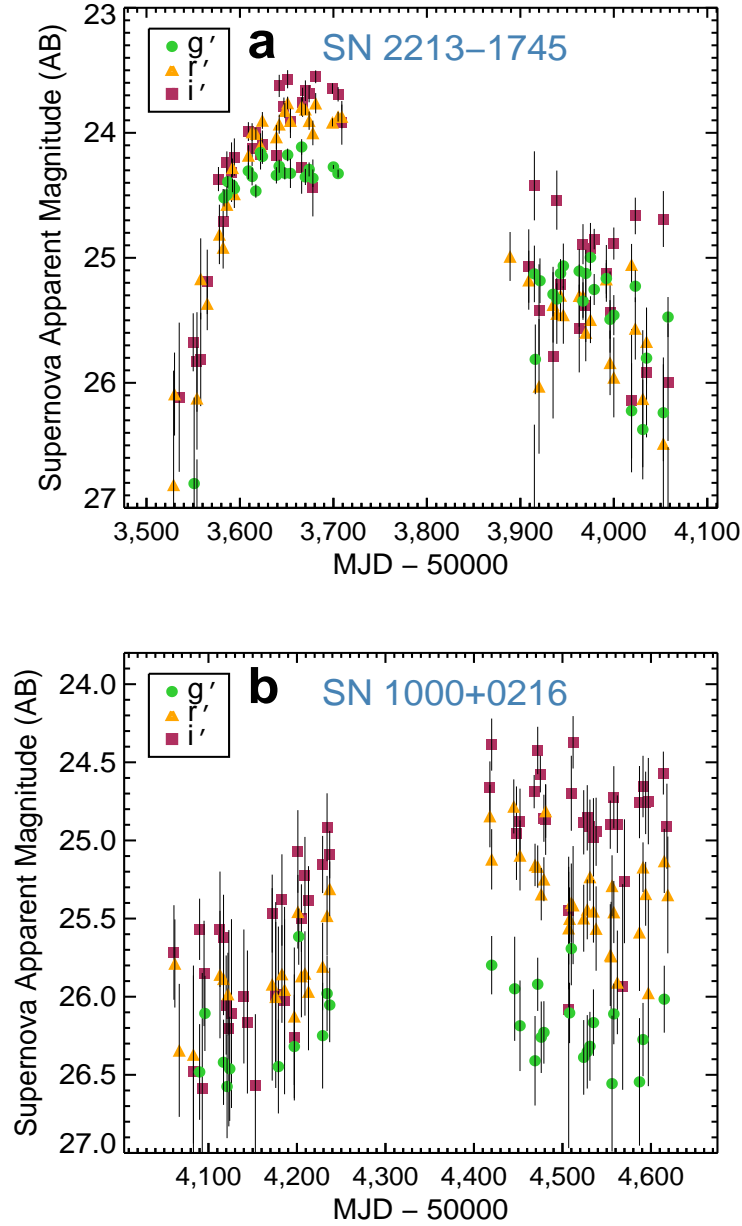
Figure 1: Light curves of high-redshift supernovae. Plotted as functions of time (MJD, modified Julian date) are the observed supernova g'-, r'-, and i'-band magnitudes and 1σ errors detected in nightly stacked images after host galaxy flux subtraction. The high quality images used in our study provide consistent and accurate photometry of the supernova host galaxies for ~6 months per year for four years (Supplementary Information, section A). **(a)** Magnitudes for SN 2213-1745 (z = 2.05) detected in deep field D4 during the observing seasons June - November 2005 and June - November 2006. The optical g'-, r'-, and i'-band data correspond to restframe far-ultraviolet continuum wavelengths of ~1,600Å, ~2,050Å, and ~2,530Å, respectively. **(b)** Magnitudes for SN 1000-0216 (z = 3.90) detected in deep field D2 during the observing seasons November 2006 - June 2007 and November 2007 - June 2008. Here, the g', r', and i' filters correspond to restframe wavelengths of ~1,000Å, ~1,300Å, and ~1,600Å, respectively. As a result, only the i' filter samples the far-ultraviolet continuum exclusively. The r' filter probes the continuum and the Lyman α (Lyα) feature and samples the decrement in flux shortward of Lyα caused by optically thick systems at lower redshift in the line of sight, termed the Lyα forest. The g' filter completely samples the spectral region of the Lyα forest to just below the Lyman limit.
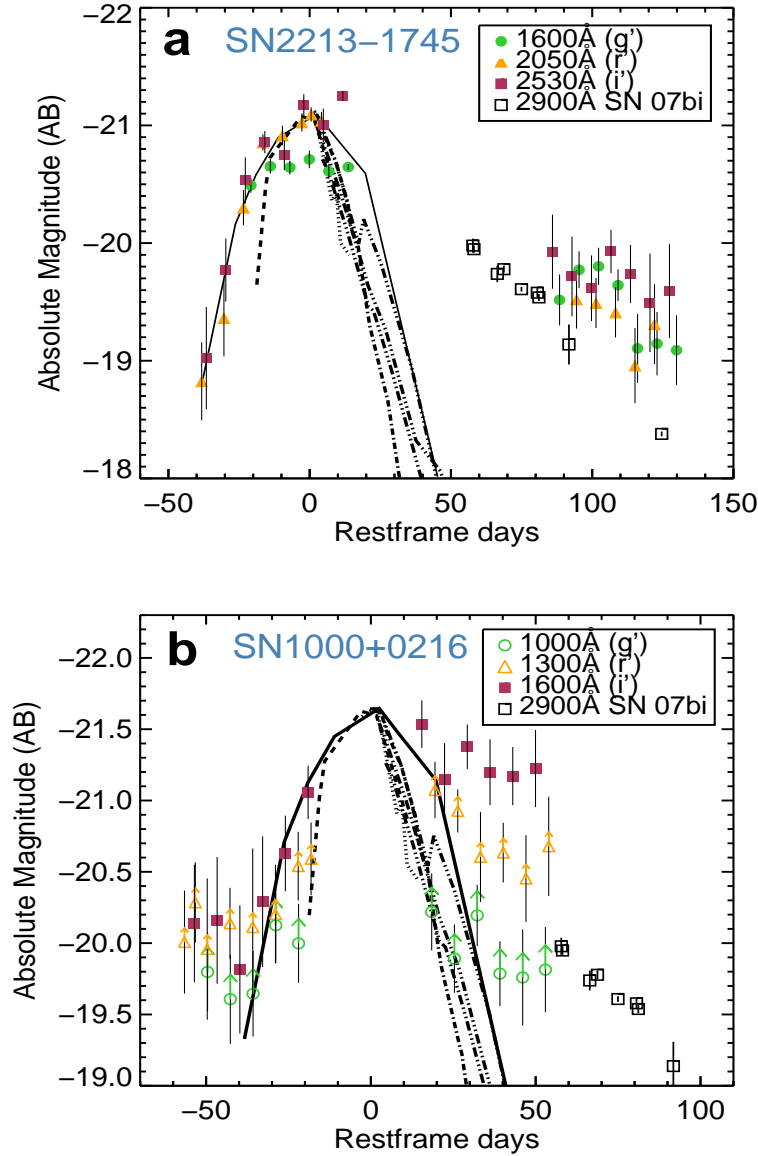
Figure 2: Absolute magnitude light curves of super-luminous supernovae. **(a)** The rise and decay of the luminosity of SN 2213-1745 in the supernova rest frame, binned in 7-day intervals. At $z = 2.05$, the g',r' and i' filters probe effective wavelengths of 1,600Å, 2,050Å, and 2,530Å, respectively. For comparison of light curve evolution, the photometry of six lower-redshift super-luminous supernovae observed at similar, but typically longer, wavelengths is overlaid and scaled by 0 - 1.2 mags to match the estimated peak light of the data: SCP 06F6[15] (SLSN-I, 3,500Å, solid curve), SN 2010gx[16] (SLSN-I, 2,900Å, dotted curve), PS1-10awh[18] (SLSN-I, 2,500Å, dashed curve), PS1-10ky[18] (SLSN-I, 2,500Å, dot-dashed curve), and SN 2008es[14] (SLSN-II, 1,700 - 2,200Å, dot-dot-dashed curves). Also shown is type SLSN-R SN 2007bi[17] with zero magnitude offset. We note that the SN 2007bi data are based on the known peak magnitude from r-band photometry acquired from just before peak to >300 days after peak.[13] Error bars on all points represent 1σ. **(b)** Same as (a) but for SN 1000+0216 at $z = 3.90$. Here, the lower redshift super-luminous supernovae are matched to an estimated peak in the i' filter (1,600Å) which is the only filter that samples the far-ultraviolet continuum of the supernova exclusively. This arbitrary peak for SN 1000+0216 results in a -0.1 to -0.6 mag offset for the lower redshift SLSNe-I and SLSN-II (as in (a), SN 2007bi is not offset). As described in Figure 1, the g' (1,000Å) and r' (1,300Å) filters partially or completely probe the spectral region of the Lyα forest. The upward arrows indicate that the true flux in these filters is higher than indicated.
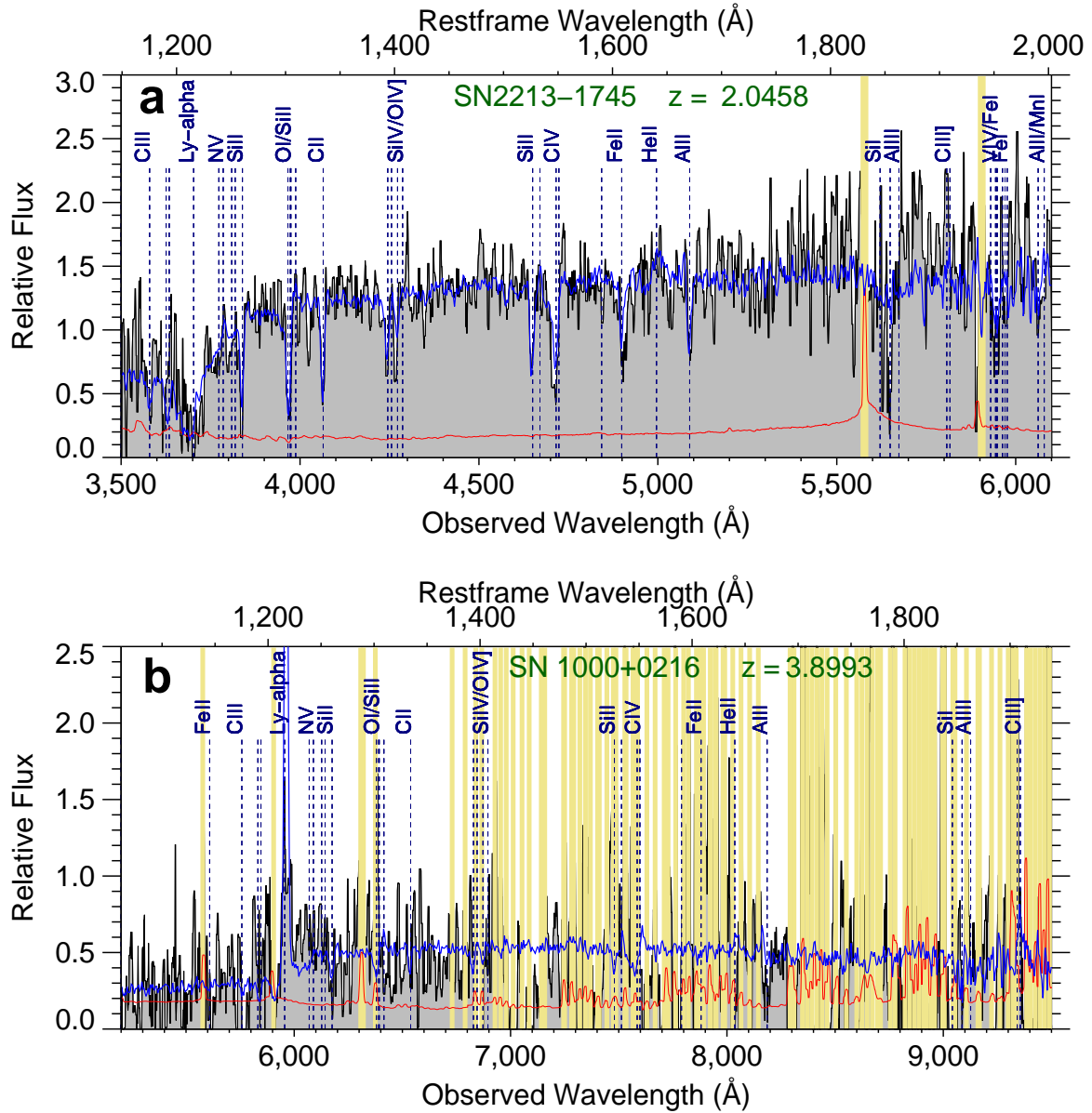
Figure 3: Late-time spectra of the supernovae and host galaxies. The spectra are shown as the dark grey filled regionS. Although Lyman break galaxies are extremely distant, they have strong absorption features and a prominent Lyα feature at 1216Å, seen in absorption and/or emission, which enable reliable identification. Labelled vertical dashed lines indicate typical atomic transitions seen in absorption. Additional absorption features may be present as a result of lower-redshift systems in the line of sight. Thick vertical light-gray lines mark the positions of bright night-sky emission lines that are difficult to remove cleanly from faint spectra. **(a)** Spectrum of SN 2213-1745 obtained 626 days (restframe) after first detection. The 1σ per pixel error array is shown by the thin black curve. A composite template of ~200 similar spectra from Lyman break galaxies (thick black curve) is overlaid and provides a secure galaxy identification and redshift. The spectrum shows no evidence of AGN activity such as strong Lyα 1,216Å, NV 1,240Å, or CIV 1,550Å emission. **(b)** Spectrum of SN 1000+0216 obtained 286 days (restframe) after first detection plotted as in (a). The poorer observing conditions and fainter nature of this object resulted in a spectrum with a lower signal-to-noise ratio in more difficulty subtracting bright night-sky lines. However, a confident host galaxy identification and redshift is achieved in part on the basis of the significant narrow Lyα emission and decrement in continuum flux shortward of Lyα as a result of the Lyα forest. Although the host galaxy exhibits narrow Lyα in emission (observed in > 50% of Lyman break galaxies), associated AGN features, such as NV 1,240Å and CIV 1,550Å, are not seen at any significance. Flux correction between ~6,300 - 6,800Å is under-represented and less reliable (Supplementary Information, section A).

Supplementary Information

Our programme searches deep, yearly stacked images for far-ultraviolet (FUV) luminous supernovae by comparing the year-to-year restframe FUV flux of $z > 2$ Lyman break galaxies (LBGs). The bulk of all FUV-luminous supernovae observed to date are type IIn supernovae and, more recently, a class of super-luminous supernovae (SLSNe) in which both are believed to result from the deaths of massive stars. Type IIn supernovae are defined by the narrow emission features in their spectra. Interaction with dense, circumstellar material results in long-lived, extremely luminous, narrow emission lines that typically remain strong for $\sim$1 - 2·(1+z) years after outburst. As a result, we follow-up supernova candidates with deep spectroscopy to identify the host galaxy redshifts and to search for late-time supernova emission.

A   Observations

Photometry We use high-quality (seeing FWHM <0.75 arcsec) images of the Canada-France-Hawaii Telescope Legacy Survey (CFHTLS) Deep fields for our photometry *(Information for the CFHTLS survey and publicly available data products can be found at a number of associated websites including http://www.cfht.hawaii.edu/Science/CFHLS/)*. LBGs are colour-selected in five bandpasses ($u^*g'r'i'z'$) in stacked images comprised of data taken over four years ($m_{lim} \sim$27) with consistent i'-band imaging[8]. Yearly stacked $g'r'i'$ images ($m_{lim} \sim$26.5) are searched for supernova-like events and consist of multiple frames taken per night over $\sim$25 - 30 nights during $\sim$6 month seasons in which the fields are observable. We focus on the $g'r'i'$ yearly stacked images because of their superior depth and even cadence as compared to the u^* and z'-bands. In addition, the Lyman limit is redshifted to the u^* and g' bands for $z \sim 3$ and $z \sim 4$ objects, respectively, and results in weak to essentially no observable flux depending on object redshift.

The rise and decay times for typical FUV luminous supernovae at $z \sim$ 2 - 4 are such that, including time dilation, they are only detectable in the integrated flux for a single $\sim$6 month observing season (or yearly stacked image). The supernovae fade sufficiently to evade detection in the following observing season due, in part, to the $\sim$6 months gap between observations. The intense luminosity and slow rise and decay of SLSNe, however, result in high redshift detections that can straddle two (or three) observing seasons. The integrated yearly host galaxy magnitudes for SN2213-1745 and SN1000+0216 and supernova magnitudes from the nightly stacked images obtained over four years are shown in Figure A.1. SN2213-1745 is not detected in the integrated flux of the host galaxy in years 2003 and 2004 and is detected at $\sim$3 - 12σ during 2005 and 2006. Similarly, SN1000+0216 is not detected in 2004/2005 and 2005/2006 and is detected at $\sim$2 - 10σ in 2006/2007 and 2007/2008. The $\sim$6 month observing seasons for the CFHTLS D2 field, in which SN1000+0216 is located, spanned November in one year through June in the next.

Spectroscopy Spectroscopic observations for SN2213-1745 and its host LBG were acquired on 03 September 2010 using the dual-arm Low-Resolution Imaging Spectrometer (LRIS)[24,30] and atmospheric dispersion corrector on the Keck I telescope. The data were obtained using a D560 dichroic and the 400 line mm^{-1} grism blazed at 3,400Å on the blue arm and the 400 line mm^{-1} grating blazed at 8,500Å on the red arm. We obtained 4 × 1,200s exposures using a 1.0 arcsec slit under good conditions and $\sim$0.8 arcsec seeing FWHM. At the time of the observations, the red arm electronics were experiencing significant problems that rendered
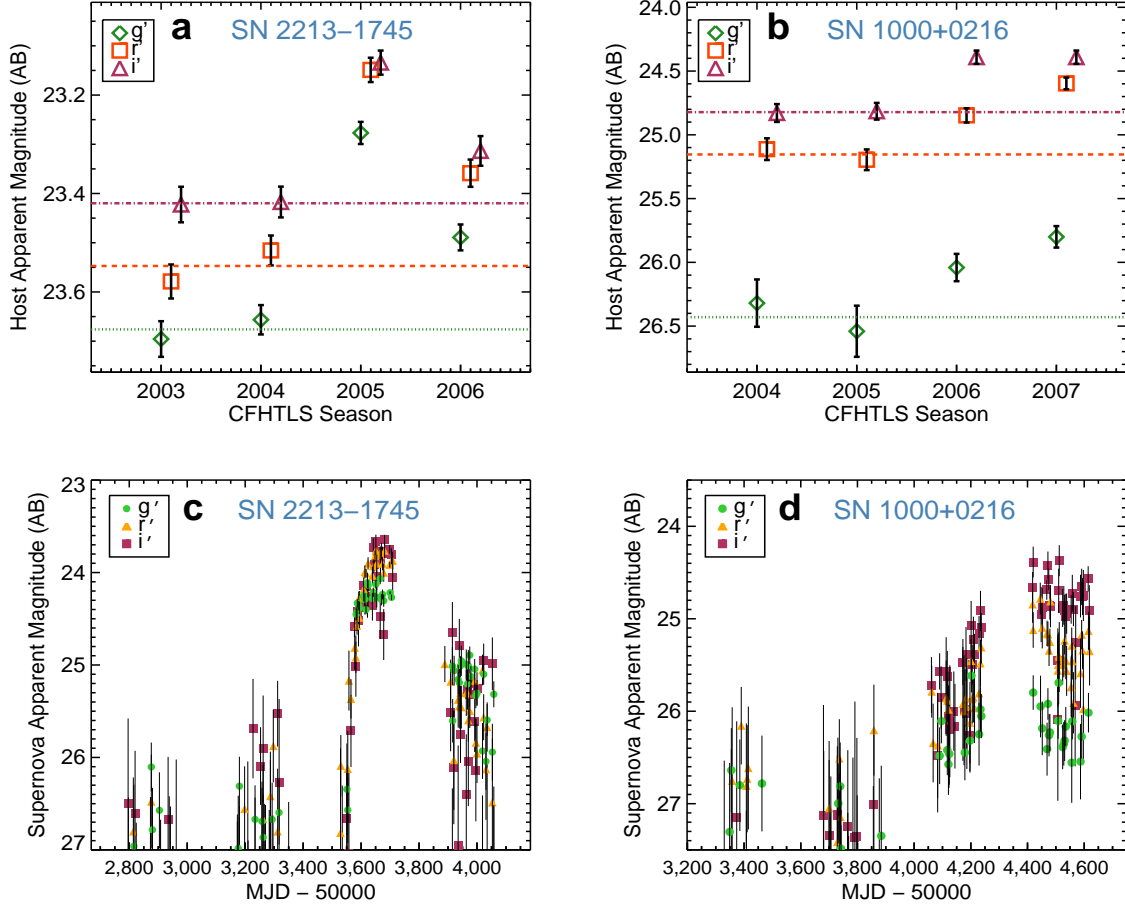
Figure A.1: Supernova and host galaxy magnitudes. **(a)** SN 2213-1745 host Lyman break galaxy magnitudes monitored over four years. The *g'r'i'* magnitudes and 1σ errors from the yearly seasonal stacked images are shown. The dotted, dashed, and dot-dashed lines mark the intrinsic host magnitude as determined from the non-detection seasons in *g',r',* and *i',* respectively. Typically, FUV luminous supernovae at $z \sim 2$ are detectable in only one year, however, SN2213-1745 was energetic enough for a significant detection in the subsequent (2006) observing season. **(b)** Similar to panel (a), but for SN1000+0216 host Lyman break galaxy. The high luminosity and high redshift of SN1000+0216 resulted in a detection in 2006 and 2007. **(c)** Nightly image stacks tracing the evolution of SN2213-1745 over four years after subtraction of the host galaxy flux. **(d)** Similar to panel (c), but for SN 1000+0216.

three quarters of the red arm CCD area suspect for scientific use. Although the spectrum was placed on the area of the CCD that was 'good', we consider any result at wavelengths greater than 5,600Å ($\sim$1,850Å, restframe) tentative. The intrinsic luminosity of the SN2213-1745 host LBG afforded a final per pixel signal-to-noise ratio of $\sim$5 - 10. Observations for SN1000+0216 and its host LBG were acquired on 10 March 2011 with LRIS using the D680 dichroic, 300 line mm^{-1} grism blazed at 5,000Å (blue arm), and 400 line mm^{-1} grating blazed at 8,500Å (red arm). We obtained $6 \times 1,200$s exposures using a 1.5 arcsec slit on a multi-object mask under moderate conditions, with $\sim$1.1 arcsec seeing FWHM and light cirrus. Because no order-blocking filter is available for LRIS on the blue arm to eliminate second-order flux from standard star observations, the flux corrections to the spectrum from $\sim$6,300 - 6,800Å are over-corrected (i.e., weaker than the true value) by a small factor. Both spectra are presented in Figure 3 in the main Letter and the spectrum of SN2213-1745 is reviewed again in Figure F.1.

Supernova location SN2213-1745 was detected in a $m_{g'}$ = 23.4 LBG in the CFHTLS Deep field D4 and SN1000+0216 was detected in a $m_{i'}$ = 24.8 LBG in Deep field D2. Figure A.2 presents small sections of the square-degree yearly stacked images centred on the host galaxies during non-detection years and images during detection years with reference images subtracted to reveal the supernovae. LBGs at $z \sim 2$ - 4 are essentially point sources in ground-based images (with some showing extended emission at $z \lesssim 2$) with average half-light radii of ~2 - 3 kpc as determined from space-based imaging.[31, 32] Our detection technique is biased towards finding supernovae within the flux extent of the host galaxies determined from the deep four-year stacked images. The physical scales at $z \sim 2$ to $z \sim 4$ range from ~8.6 to ~6.8 kpc arcsec^{-1} and the plate scale of CFHTLS MegaCam imager is 0.187 arcsec pixel^{-1}, corresponding to ~1.3-1.6 kpc pixel^{-1} over the redshifts of interest here. We note that the separations in our full sample to date of 12 $z > 2$ FUV-luminous supernovae range from ~0 - 3 kpc, physical, and are consistent with this expectation.

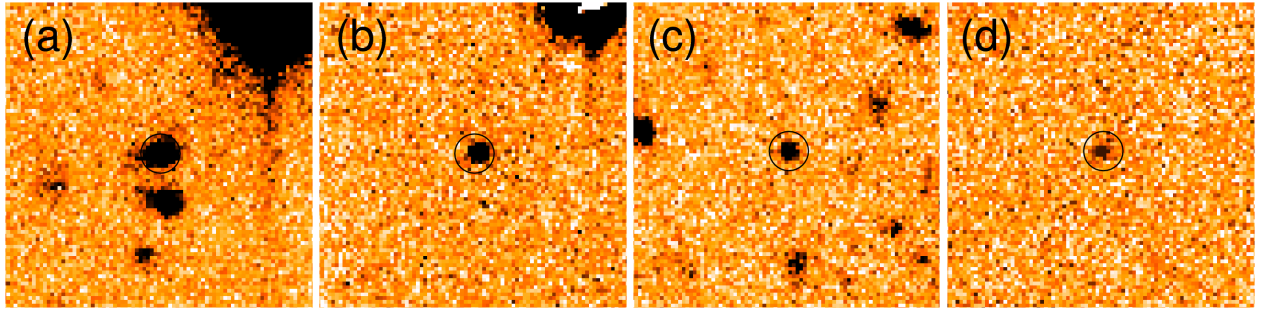
Figure A.2: Thumbnail r'-band images of the supernovae and their host galaxies. All images are centred on the host galaxy FUV centroid and are 15 arcsec on a side oriented with North upward and East to the left. **(a):** The SN2213-1745 host galaxy in non-detection season 2004. The nearby companion galaxy to the South has the same redshift within the uncertainties and a projected separation of 21 kpc, physical (§E). The proximity of this galaxy and the faint extended features of the two galaxies suggest that they are interacting. The circle is placed on the host galaxy FUV centroid and has a radius of 1 arcsec. **(b):** Image of SN2213-1745 in the first detection season 2005 after subtraction of the reference image. The high-quality CFHTLS yearly stacked images enable clean subtraction images; only the saturated bright, $m_{r'}$ = 16.7, star in the upper right hand corner cannot be well-subtracted. The circle helps to visualise the potential small offset (~1 kpc, physical) of the supernova with respect to the host galaxy centroid. **(c) & (d):** Thumbnail images similar to (a) & (b) but for the SN1000+0216 host galaxy in non-detection season 2005/2006 (c) and detection season 2007/2008 (d).

The superb CFHTLS image astrometry enables relative centroid accuracies of ~0.04 pixels (*http://www3.cadc-ccda.hia-iha.nrc-cnrc.gc.ca/community/CFHTLS-SG/docs/quality/astrometry.html*) and we find that the relative supernova-host galaxy centroid measurements season to season and filter to filter are accurate to $\lesssim0.5$ pixels[8] over the full square degree images. The relatively central location of the host LBGs in each field, where astrometric solutions are typically more accurate, produces centroid accuracies of ~0.3 pixels. Centroid separations are measured for each filter between the host centroid in the two non-detection years and the supernova centroid in the two detection years. The measurements produce consistent centroid separations, with an average $g'r'i'$ separation of 0.52 ±0.34 kpc, physical, for SN2213-1745. The small separation is consistent with zero considering the uncertainties, however, the centroid offsets appear in the same direction (West) for all 12 measurements with all errors being consistent. The average $g'r'i'$ separation for SN 1000-0216 is 0.62 ±0.57 kpc and consistent with zero.

Here, the offsets appear in the same direction for the three filters again, but this time to the South East. However, the g'-band detection is very weak owing to the effects of the Lyα forest and the Lyman limit.

Taking the separations measured from the images at face value, the two SLSNe appear to reside at, or near, their apparent host centres. The two SLSN host galaxies are more luminous than average LBGs in our sample at the respective redshifts and SLSNe residing near the host nuclei of luminous host galaxies is a topic of discussion for low redshift events[2,33]. However, we note two important points. Firstly, the image separations are projected separations in the plane of the sky, thus the true three-dimensional separations between the LBGs and supernovae are equivalent to, or larger than, the projected separations. Secondly, the images probe the restframe FUV that traces high star formation regions in the relatively young, high redshift galaxies. Such regions are typically clumpy and may, or may not, occur at the host centre or appear symmetric in intensity about the host centre. Although the supernova centroids are reliable, the host galaxy centroids measured from the images are less so. As a result, the image separations presented here should be considered indicative as opposed to definitive.

B   Rates

As discussed in the main Letter, SLSNe are classified into three types, SLSN-I that show no hydrogen, SLSN-II that are hydrogen rich, and SLSN-R that are powered by ^{56}Ni decay and are likely pair-instability supernovae. The SLSN rate at low to intermediate redshift is estimated to be $\sim 10^{-8}$ h_{71}^3 Mpc^{-3} yr^{-1}, in which ~ 0.2 are SLSN-R candidates[1,2]. This rate is to be compared to 10^{-4} h_{71}^3 Mpc^{-3} yr^{-1} for the full set of core-collapse supernovae[34,35] ($\gtrsim 8$ $M_\odot$ progenitors).

We search for SLSNe in LBGs over four redshift paths, $z \sim 2$, $z \sim 3$, $z \sim 4$ and $z \sim 5$, using standard colour-selection techniques[22-24] tailored to the CFHTLS Megacam filters. We map the evolution of 10 starforming and passive galaxy templates from $z = 0$ - 6 in various colour-colour planes to efficiently ($\gtrsim 90\%$) select LBGs at the desired redshifts that are con-firmed from >100 LBG spectra acquired specifically for this programme. Relevant to the two discoveries presented here, the colour-selection probes $\delta z \sim 0.6$ at $z \sim 2$ and $z \sim 4$. Com-puting the effective area of the images and correcting the redshift paths by the $z \sim 2$ and $z \sim 4$ photometric selection functions results in volume of $\sim 6 \times 10^6$ h_{71}^{-3} Mpc^3 at both redshifts, adopting an $H_0 = 71$, $\Omega_\Lambda = 0.73$, $\Omega_M = 0.27$ cosmology.

The high redshift volumetric rate is estimated by simulating the rapid evolution of SLSN-I and SLSN-II luminosity profiles and slower evolving SLSN-II with interaction and SLSN-R profiles at the two redshifts. We convolve the supernovae with the detectability window functions (that extend beyond the formal four observing seasons) and use the requirement that supernovae need only one season detection. Using the specifics of the survey and the four fields, the one $z \sim 2$ detection implies a rough SLSN volumetric rate of $\sim 4 \times 10^{-7}$ h_{71}^3 Mpc^{-3} yr^{-1}. The single $z \sim 4$ detection, along with the competing effects of shorter time, restframe, sampled by the CFHTLS photometry and shorter gaps in coverage produces a similar rate of $\sim 4 \times 10^{-7}$ h_{71}^3 Mpc^{-3} yr^{-1}. We note that because our supernovae are detected in the FUV, the estimated high redshift rate reflects a lower limit. FUV radiation is highly susceptible to extinction from metal-line absorption and dust in the local environment of the supernovae, the interstellar medium of the host galaxies, and the circum-galactic and intergalactic medium. Thus, there may be a significant fraction of SLSNe with escaping FUV flux that falls below our detection threshold.

The rate of core-collapse supernovae closely follows the star formation rate over cosmic time because of the short lifespans of massive stars. The core-collapse supernova rate is expected to increase by a factor of ~5 from $z \sim$ 0.3 - 2,[34,35] following the evolution in the cosmic star formation rate, and then remain relatively constant or experience a decline to $z \sim$ 4.[36,37] The rate of high-redshift SLSNe based on our two FUV detections, uncorrected for FUV extinction, is an order of magnitude higher than the rate of SLSN at low redshift, after correcting for the expected $\gtrsim$5 increase as a result of increases star formation. Our rough high redshift SLSN rate provides the first direct evidence that the number of massive stars in the early Universe may be higher than that observed at low redshift.

C   Light curves

To generate the supernova light curves for each filter, we use the technique of point-spread function (PSF) photometry on image subtractions. We first construct a reference image from data where no supernova light is expected (2003 for SN2213-1745 and 2004 for SN1000+0216). The reference image is then subtracted from each image where the supernova light is present using a PSF matching technique, removing the host galaxy light and leaving only the supernova light in the difference image. The supernova photometry is then measured with a PSF-fitting technique that uses the PSF measured from nearby field stars.[38] The photometric data are calibrated using a set of tertiary standard stars.[39] The photometry for SN 2213-1745 and SN1000+0216 is listed in Tables F.1 and F.2.

Rise times The photometric data points and the limits imposed by the non-detections in previous seasons indicate ~50 to >150 day rise time from outburst to peak magnitude for the two supernovae. As an exercise to help narrow the rise time range and possibly shed light on the nature of the supernovae, we first follow a conventional approach and fit low order polynomials to the slowly evolving photometric data. The polynomial fit approach estimates the date of outburst and rise time to peak without any assumptions of the progenitor however, for the CFHTLS seasonal data, has difficulty fitting the evolution over the ~6 month periods, observed frame, in which the supernovae were not observed. The peak magnitudes are not well constrained within the coverage gaps and it is unclear whether the peak for SN1000+0216 falls within the gap or occurs beyond the extent of the data. As a result, the polynomial fit rise times are rough estimates and defined here as the time for the supernovae to rise 5 magnitudes to peak as determined by the functional fit. Figure C.1 displays the polynomial fits for both supernovae. In addition, because the high redshift supernova data follow the behaviour of low-redshift SLSNe-R (see main Letter), we compare their light curve evolution to pair-instability supernova models.

Polynomial fits The polynomial fits to the SN2213-1745 *g', r',* and *i'* data separately produce very similar results, but the lack of data constraints during rise for the *g'* data yields a significantly slower rise time (>200 days) for a third order polynomial. Because the *r' and i'* data follow a similar evolution over the date ranges probed by each filter, the values reported here are those fit to the combined data from the *r' and i'* filters. The SN2213-1745 *r'i'* data are fit with third, fourth, and fifth order polynomials and result in rise times of 81, 62, and 64 days, respectively. We note that these rise times are a lower limit to the true value when considering that the observational gap of photometric coverage occurs after these estimated dates of peak magnitude. We adopt an intermediate polynomial fit rise time of 70 days for this supernova.
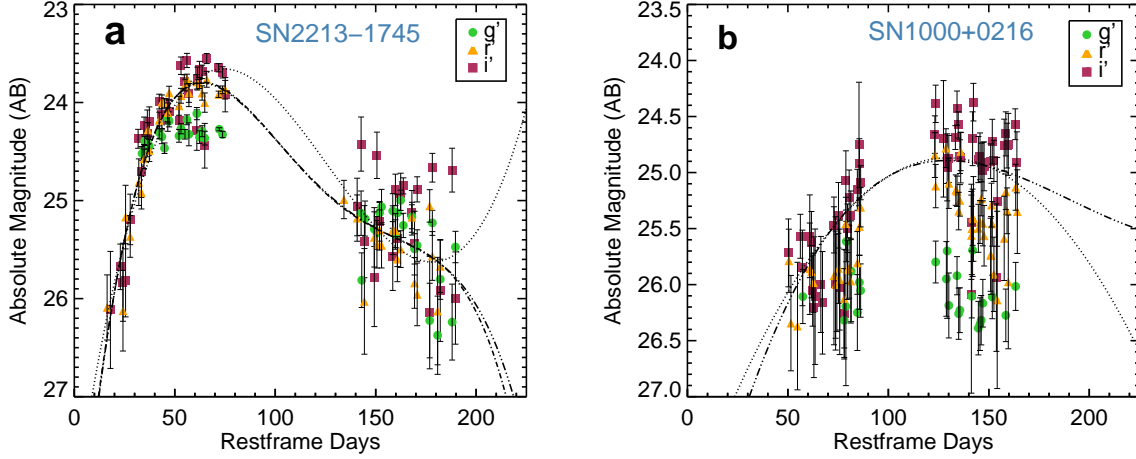
Figure C.1: Polynomial fits to the nightly stacked image photometry for the two high redshift supernovae. The gap in coverage between observing seasons alters the shape of the polynomial and makes the determination of the time of peak magnitude less reliable, particularly in the case of SN 2213-1745 which exhibits a larger change in magnitude over a larger number of restframe days. **(a):** The photometry of SN2213-1745 is shown fit with third (dotted curve), fourth (dot-dot-dash curve), and fifth (dot-dash curve) order polynomials. **(b):** Similar to panel (a), but for SN1000+0216. Because of the effects of the Lyα forest and the Lyman limit on the g' and r' filters, only the i'-band that probes the supernova continuum is fit. The results from second (dotted curve) and third (dot-dash curve) order polynomial fits are shown.

Second and third order polynomial fits to the i' filter data of SN1000+0216 result in rise times of 146 and 129 days, respectively (higher polynomials were unconstrained at early times). Second and third order fits to the g' filter appear identical, with each producing rise times of 134 days. A second order fit to the r' filter produces a rise time of 138 days with the third order fit unconstrained at early times. The g' and r' fits are not shown in Figure C.1 for clarity. If we assume that the true peak magnitude occurs between detection seasons, the non-detection in the previous season places an upper limit on detection to $\sim$130 days. Otherwise, the rise time is >150 days if the peak occurs beyond the data. Given that the g' and r' filters probe the Lyα forest and are detected at lower significance, we focus on the fits to the i' filter and adopt a polynomial rise time of 129 days.

Pair-instability supernova models Stars with masses between 140 - 260 $M_\odot$ are theorised to end their lives as pair-instability supernovae (PISNe).[4-6] The high temperatures and relatively low densities that develop in the cores of such massive stars promote electron-positron pair production. The rapid conversion of pressure-supporting radiation into rest-mass in such a core leads to a hydrostatic instability that can trigger a run-away nuclear explosion that completely obliterates the star. PISNe produce peak energies of $\gtrsim 10^{44}$ erg and exhibit a slow light curve evolution consistent with the radiative decay of ^{56}Ni. Because this behaviour is similar to that of our high redshift SLSNe, we compare their FUV evolution to that of radiative hydrodynamics PISN simulations.[19]

We find that 150 - 250 $M_\odot$ low-metallicity stellar models that retain their hydrogen envelopes (blue and red supergiant models) evolve too slowly to peak luminosity ($\gtrsim$200 days) and/or have too low FUV energies to provide a reasonable fit to the data. We note that we cannot
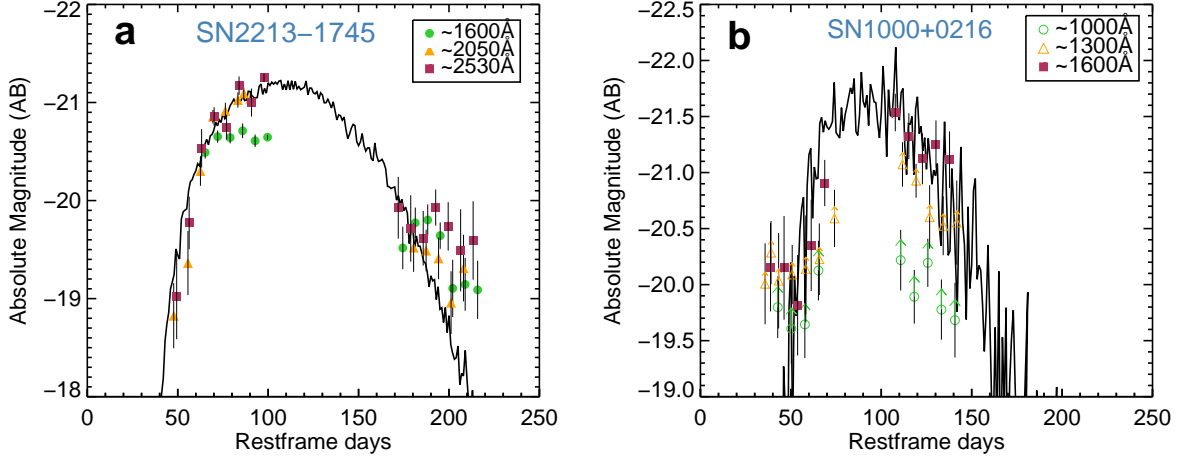
Figure C.2: Comparison of the data to the time evolution of a pair-instability supernova model. **(a)** The rise and decay of SN2213-1745 binned in 7-day intervals. The overlaid curve is the far-ultraviolet evolution of a 130 $M_\odot$ bare helium core pair-instability supernova model averaged over the restframe continuum near 2000Å as sampled by the observed *r'* bandpass and offset to match the luminosity of the data *(see text)*. **(b)** Similar to panel (a) but for SN1000+0216. Because the *g'* and *r'* filters probe the Lyα forest and are subject to significant absorption by gas from lower redshift systems in the line of sight (the true flux is higher as denoted by the upward arrows), the model is averaged over the restframe continuum near 1600Å as sampled by the observed *i'* bandpass. The supernovae appear to follow the far-ultraviolet evolution of the model well, however the higher luminosity of the data may point to either model limitations or a different (or additional) luminosity mechanism.

rule out the more luminous supergiant models for SN1000+0216 if the peak occurs beyond the extent of the data. We find good fits to a 130 $M_\odot$ bare helium core model that follows the evolution of progenitor star with an initial mass of $\sim$250 $M_\odot$ with its outer envelope, consisting largely of hydrogen, removed from binary mass exchange or stellar evolutionary processes.

The evolution of SN2213-1745 follows the form of the bare helium core model well, as seen in Figure C.2, and does so for the model integrated over each of the restframe wavelength ranges that corresponding to the the *g',r',* and *i'* filters; 1600Å $\pm$240 (*g'*), 2060Å $\pm$200 (*r'*), and 2550Å $\pm$250 (*i'*). The model suggests a rise time of $\sim$105 days, however, the supernova is more luminous than expected by a factor of 2.8, 1.9, and 0.7 for the *g',r',* and *i'* filters, respectively. Although the model is the state-of-the-art for PISN simulations, it remains less well constrained in the FUV. The higher luminosity and bluer colour of SN2213-1745 may be a result of higher photospheric explosion temperatures and/or simulation limitations. The model resolution for the shorter wavelengths probed by SN1000+0216 data is more limited. We integrate the model over the longer wavelengths probed by the *i'* filter, 1600Å $\pm$150, that samples the supernova continuum and avoids the effects from the Lyα forest and Lyman limit. We find that SN1000+0216 appears to follow the evolution of the model reasonably well, peaking at $\sim$95 days after outburst, but it is $\sim$2 mag more luminous.

From the PISN model, a low-order polynomial fit to the data, and the constraints set by the previous season non-detections, we estimate a 75 – 125 day rise time from outburst to peak magnitude for SN2213-1745 and 95 – 130 days for SN1000+0216.

D   Nature of the High-Redshift Super-luminous Supernovae

In an attempt to understand the nature of the high redshift SLSNe, it is important to keep in mind that the light curves of the supernovae do not match the quicker fade rates of SLSN-I or SLSN-II at low and intermediate redshift (cf. Figure 2, main Letter). Moreover, our SLSNe are observed in the FUV where the fade rates are expected to evolve quicker than the near-UV and optical. Instead, the evolution of the two high redshift supernovae provide a good match to that of SLSN-R and the 0.0098 mag day^{-1} decay rate of ^{56}Co (daughter product of ^{56}Ni) out to the extent in which light curves are sampled. We find that the observed high FUV luminosities may push the supernovae beyond the energies possible for the PISN interpretation of SLSN-R as estimated by the bare helium core model discussed in the previous section, in particular for SN1000+0216. A possible alternative and/or additional source for late-time emission is the interaction of the supernovae with previously expelled circumstellar material (§F).

One plausible interpretation for the high redshift SLSNe is that they are examples of pulsational pair supernovae. Stars in the mass range $\sim$80 - 150 $M_\odot$, depending on rotation rate, metallicity, and other parameters, may experience pulsational pair instability and fail to completely explode on their first try.[40] During the evolution of a star this massive, the core becomes pair-instable and the explosion ejects many solar masses of outer envelope material but the energy is insufficient to unbind the star. The core stabilises again, contracts, and grows hotter. A subsequent pair-instability pulsation drives off additional material at higher velocities than the first ejection that collides with the originally expelled material, leading to an extremely luminous event[19]. The expected higher rate of pulsational pair-instability supernovae as compared to PISNe is more consistent with our rough rate estimate, given the acceptable mass range of each population, however, such events do not generate the large amounts of ^{56}Ni needed to power the observed late-time luminosity. Similar to type IIn supernovae, collision of shells of material could, in principle, provide an additional late-time luminosity contribution and generate shock-induced emission that persists to late times. Evidence for long-lived circumstellar interaction-induced emission features can be detected in deep, late-time FUV spectroscopy in some cases and is discussed in §F.

E   Host galaxies

SN2213-1745   The host galaxy to SN 2213-1754 is a luminous, M_{FUV} = -21.4, $z \sim 2$ LBG. The star formation rate (SFR) of the host galaxy based on the restframe FUV (AB)[10,11] magnitude derived from the observed g' band (restframe $\sim$1600Å) magnitude, is estimated to be $\sim$20 $M_\odot$ yr^{-1} when using the simple relationship, SFR = 6 $\times$ 10$^{-(8+0.4\,M(FUV))}$ $M_\odot$ yr^{-1}, that ignores the effect of dust.[36,41] The host was densely monitored photometrically for four observing seasons and generated a single supernova-like outburst. The host spectrum shows features that are representative of typical LBGs, including a strong Lyα absorption feature similar to that seen in $\sim$25% of the LBG population, and no features typically attributed to AGN. An LBG composite template gives a very good fit to the spectrum as seen in Figure F.1.

The object located 2.45 arcsec (20.7 kpc at $z \sim 2$) to the South of the SN2213-1745 host galaxy (see Figure A.2) has a similar apparent magnitude, m$_{r'}$ = 23.8, and is also a colour-selected $z \sim 2$ LBG. The spectroscopic observations for the SN2213-1745 were executed such that the longslit was oriented to simultaneously obtain the flux from the nearby object. The observations were done without loss of wavelength-dependent flux, which could occur if the

orientation of the two objects is not optimal with the parallactic angle, because the atmospheric dispersion corrector on LRIS was deployed. The spectroscopy confirms the object as an LBG with redshift z = 2.0455 $\pm$0.0008. Inspection of the flux contours of the CFHTLS images reveals diffuse flux extending to the East of the two LBGs similar to the appearance of tidal tails, providing evidence that the two galaxies are interacting. Galaxy interactions induce the collapse of cold gas and trigger star formation in galaxies and associated gas clouds.[42–44] The star forming episodes that result from interactions increase the chance of observing the deaths of short-lived very massive stars.

SN1000+0216 The host to SN1000+0216 is a luminous, M_{FUV} = -21.2, $z \sim 4$ LBG. Using the SFR relationship above, the similar FUV luminosity to SN2213-1745 (derived from the observed i'-band magnitude, restframe $\sim$1600Å at $z \sim 4$, similarly produces a FUV SFR of $\sim$20 $M_\odot$ yr^{-1}. The host exhibited a single supernova-like outburst over the four years monitored and we see narrow Lyα in emission that is common to $\gtrsim$50% of the LBG population, and no associated emission attributable to AGN activity. Finally, there is no clear evidence for galaxy interaction as there is for the host of SN2213-1745. We note that the depth and resolution of the data are not sensitive to late stages of interaction, interactions with minor companions (approximately 5:1 or less mass) which are more common, or interaction with companions that are not currently undergoing starbursts (e.g., on their first pass) and thus do not produce strong FUV flux as is witnessed for low-redshift LBG analogues.[45–47]

SLSNe-R and Population III star hosts Theory states that massive stars form more easily in regions of low-metallicity whereas Population III stars form in regions of essentially zero metallicity. At low redshift, the environments that best suit the necessary conditions for massive star formation may be low-luminosity, low-metallicity star forming dwarf galaxies. Indeed, low-redshift SLSNe, including SLSNe-R, are found in star forming galaxies with luminosities -16 < M < -21, with two luminous exceptions, SCP 06F6 and SN 2006gy.[48] In addition, the hosts have relatively low metallicities (where measured) and high specific star formation rates (star formation rate per unit galaxy stellar mass). The low-redshift SLSN-R SN 2007bi was detected in a faint (M_B = -16), star forming host galaxy[13] with estimated low metallicity ($\sim$ 0.3 solar)[17].

Our high-redshift supernova hosts are star forming galaxies residing at the luminous end of the low-redshift SLSN host galaxy luminosity distribution.[48] We remark that our survey is not sensitive to host galaxies with $M_{FUV} \gtrsim$ -19.5, but a search for high redshift 'orphan' supernovae, events whose host galaxy is below the detection threshold of the survey, is in progress. Our FUV data alone do not provide reliable metallicities for our supernova hosts but the typical metallicities of LBGs measured using infrared (restframe optical) spectroscopic diagnostics are low, $\sim$0.5 - 0.1 solar.[47] Finally, the two high redshift supernova hosts have high specific star formation rates which is a ubiquitous feature of the LBG population. Thus, the low metallicities and high specific star formation rates are consistent with low redshift SLSN-R hosts, but the relatively high luminosities of the high-redshift host galaxies would seem at odds with that of SN 2007bi. However, it is unlikely that the potential low-redshift preference for faint SLSN-R hosts similarly holds at high redshift where typical galaxies have low-metallicities and high star formation rates, thus higher intrinsic luminosities.

The many ISM metal absorption lines in our deep spectra reveal that the globally averaged metallicity of the high redshift supernova host galaxies is not primordial. Consequently, in order for the supernovae to be Population III stars, they would need to have formed in pockets of pristine gas. This could occur either within the galaxies (e.g., the enrichment of metals

in the galaxies is clumpy), in the low metallicity environment of the galaxy haloes, or in sub-haloe galaxies or line-of-sight gas clouds in the host vicinity. Finally, we note the possibility for SLSNe to form as a result of a collision of two stars in young, dense star clusters in the host galaxies.[49] The clumpy star forming nature of LBGs could provide a environment that is conducive to stellar collisions, although this type of event is predicted to be ~100 times more rare than our estimated rate.

F Supernova late-time emission

As discussed above, the interaction of circumstellar material may be a mechanism to contribute to the luminosity of SLSNe. One example is SN 2006gy, a SLSN-II at low redshift, that exhibited circumstellar interaction and may be an example of a pulsational pair-instability event.[40] Such interactions may produce FUV emission features that are similar to the long-lived features observed in local type IIn supernovae.[50,51] Our survey for FUV-luminous supernovae at high redshift has detected type IIn-like emission features in several of our confirmed $z \gtrsim 2$ supernova spectra. In this section, we outline our approach to search for late-time emission in high redshift supernova spectra.

LBGs exhibit a prominent Lyα feature observed in absorption, emission, or a combination of both. Apart, from Lyα, LBGs show no significant emission lines over the wavelengths studied other than weak HeII 1,640Å and CIII] 1,909Å that appear in some spectra. Our approach is to investigate any excess emission features in our LBG hosts, particularly at atomic transitions seen in low-redshift FUV supernova spectra that exhibit late-time circumstellar interaction. Features include Lyα 1,216Å, NV 1,240Å, OI 1,358Å, OIV 1,400Å, NIV] 1,486Å, excess CIV 1,550Å, NIII 1,753Å, SiII 1,808Å, NeIII] 1,815Å, SiIII] 1,883Å, and excess CIII] 1,909Å. An important consideration is that the peaks of many circumstellar interaction emission features in low-redshift spectra are blueshifted by ~1000 - 4000 km s^{-1} and can appear relatively broad. Moreover, because the high redshift spectra include the entire flux from the host, any supernova features are affected by interstellar medium absorption features of the host that can significantly alter the final observed profile. This differs from low redshift where the host galaxy contamination in supernova spectra is small. Our programme includes future spectroscopy of host galaxies having candidate supernova emission to confirm or refute any potential detections by the decay, disappearance, or continued presence of the lines.

In an effort to isolate potential late-time supernova emission, we subtract matched composite spectra from the host galaxies. The composite spectra are constructed from 200 $z \sim 3$ LBGs selected based on the observed relationships between Lyα equivalent width, FUV continuum, and ISM absorption line profiles[52]. As seen in Figure F.1, the composite spectrum provides an excellent fit to the relatively high signal-to-noise ratio continuum and prominent features of the host galaxy to SN2213-1745. We note that several absorption features are seen in the data, that are not seen in the template, that result from metal line absorption from lower redshift systems in the line of sight. These features are also seen in the difference spectrum shown as the green curve with white fill in the figure. Although additional absorption features are expected, additional emission features are not.

The SN2213-1745 host galaxy exhibits strong Lyα absorption, similar to that seen in ~25% of the LBG population, and little evidence for hydrogen emission from the supernova that would classify this event as a SLSN-II. Although the host LBG might absorb a significant fraction

of the Lyα emission, the expected broad nature of the feature as seen in low-redshift type IIn supernova spectra would predict a leakage of measurable fraction of emission given the expected clumpy distribution of neutral hydrogen in the host. The lack of Lyα emission provides spectroscopic evidence against a SLSN-II classification, independent of the mismatch between the light curve evolution of low redshift SLSN-II and SN2213-1745, and further supporting a SLSN-R interpretation.

The SN 1000+0216 host galaxy exhibits Lyα in emission, common to ≳50% of the LBG population (see Figure 3, main Letter). The lower signal-to-noise ratio and fluxing caveats (§A) of the existing data does not allow a similar difference spectrum analysis to that of SN2213-1745. As a result, it is currently unclear whether any excess emission from the supernova is present in the form of a contribution to the Lyα feature or other FUV emission lines typical of circumstellar interaction. Additional spectroscopy of SN1000+0216 and future spectroscopy (>3 years post-detection, restframe) of both supernovae will enable a more comprehensive late-time emission analysis.
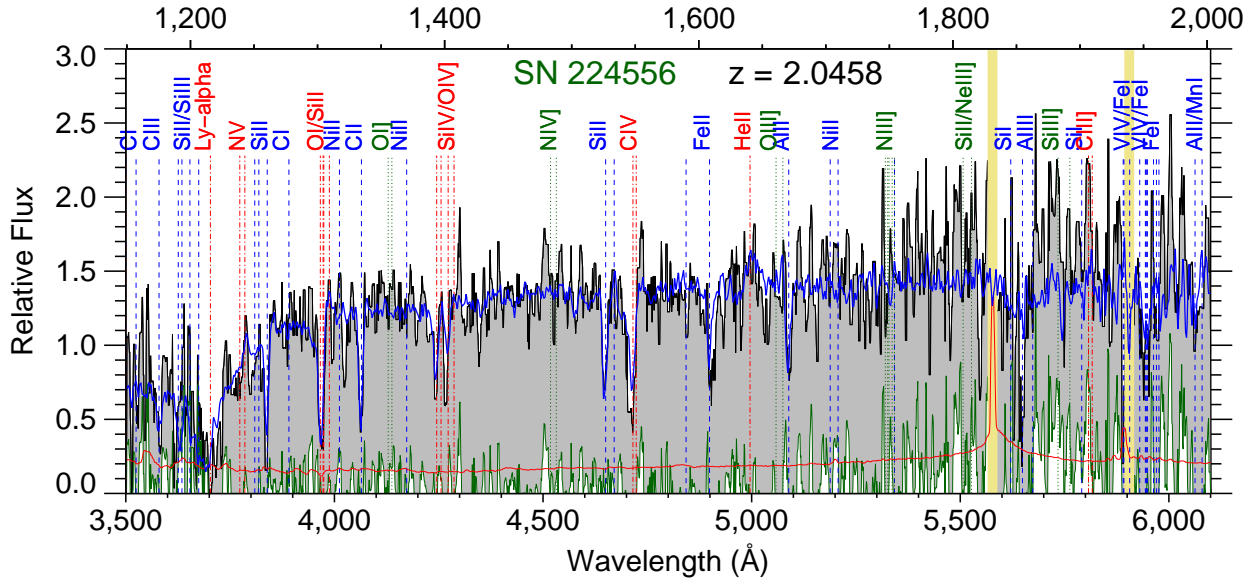
Figure F.1: Late-time host galaxy spectrum similar to Figure 3 in the main Letter. SN2213-1745 host galaxy spectrum (black curve with gray fill) is shown smoothed by 5 pixels. Labelled vertical (blue) dashed lines indicate typical atomic transitions seen in absorption in LBGs. Vertical (green) dotted lines mark late-time transitions observed in low-redshift supernovae exhibiting circumstellar interaction and are not observed in LBGs and red (dot-dashed) lines denote transitions seen in both LBGs (typically in absorption) and supernovae (in emission). The host galaxy error array is shown as the thin red curve and thick vertical (yellow) lines mark the positions of bright night sky lines. The difference spectrum, after the subtraction of the composite spectrum from the data, is shown as the (green) curve near zero with white fill. As noted in the text, additional absorption features in the difference spectrum is expected as a result of lower redshift systems in the line of sight, but additional emission features are not. The lower signal-to-noise ratio and fluxing caveats (see text) of the existing SN1000+0216 data does not enable a similar difference spectrum analysis.

day (MJD)	g'	error	day (MJD)	r'	error	day (MJD)	i'	error
53551	26.80	0.68	53529	26.81	0.91	53535	26.11	0.59
53554	27.17	0.55	53530	26.08	0.33	53550	25.67	0.23
53583	24.52	0.06	53535	29.42	2.15	53554	25.83	0.39
53586	24.49	0.06	53554	26.12	0.41	53558	25.81	0.37
53587	24.39	0.04	53558	25.16	0.32	53565	25.19	0.25
53592	24.42	0.05	53565	25.36	0.21	53577	24.37	0.09
53594	24.44	0.07	53578	24.81	0.23	53582	24.70	0.25
53609	24.30	0.06	53582	24.91	0.16	53586	24.23	0.09
53613	24.34	0.07	53586	24.57	0.09	53591	24.31	0.23
53617	24.46	0.05	53592	24.27	0.07	53594	24.19	0.14
53622	24.15	0.06	53594	24.48	0.11	53609	23.99	0.07
53624	24.18	0.05	53609	24.18	0.08	53613	24.12	0.13
53639	24.33	0.06	53613	23.99	0.07	53617	23.99	0.04
53642	24.26	0.05	53617	24.00	0.04	53622	24.17	0.12
53648	24.32	0.04	53622	24.10	0.09	53624	24.09	0.11
53651	24.17	0.05	53624	23.90	0.06	53639	24.17	0.14
53654	24.32	0.11	53639	24.03	0.09	53642	23.62	0.08
53666	24.11	0.06	53642	23.93	0.07	53647	23.78	0.07
53670	24.35	0.06	53648	23.82	0.06	53651	23.57	0.07
53674	24.29	0.05	53651	23.76	0.05	53654	23.91	0.12
53678	24.36	0.07	53654	23.90	0.09	53666	24.28	0.20
53700	24.27	0.01	53666	23.78	0.07	53667	23.75	0.11
53705	24.32	0.03	53670	23.81	0.04	53670	23.66	0.08
53915	25.12	0.22	53674	23.90	0.07	53674	23.68	0.06
53916	25.81	0.27	53678	24.00	0.09	53678	24.44	0.22
53921	25.18	0.17	53681	23.76	0.08	53681	23.55	0.05
53935	25.29	0.17	53699	23.91	0.03	53699	23.64	0.04
53939	25.32	0.16	53705	23.87	0.03	53705	23.69	0.05
53943	25.12	0.11	53709	23.86	0.09	53709	23.92	0.17
53946	25.06	0.17	53889	24.98	0.19	53909	25.06	0.29
53963	25.10	0.17	53909	25.17	0.23	53915	24.42	0.27
53967	25.34	0.15	53915	27.40	1.07	53920	25.41	0.36
53970	25.12	0.18	53920	26.02	0.53	53935	25.78	0.49
53975	24.99	0.10	53935	25.37	0.30	53939	24.53	0.23
53979	25.25	0.12	53939	25.44	0.24	53943	25.21	0.19
53992	25.16	0.12	53943	25.30	0.20	53963	25.56	0.35
53996	25.49	0.15	53946	25.45	0.23	53967	24.89	0.16
54000	25.45	0.16	53963	25.30	0.24	53970	25.38	0.28
54019	26.22	0.38	53967	25.30	0.17	53975	24.92	0.20
54023	25.22	0.12	53970	25.59	0.22	53979	24.85	0.08
54031	26.37	0.39	53975	25.49	0.18	53992	25.12	0.22
54035	25.80	0.20	53992	25.17	0.15	53996	25.43	0.32
54053	26.23	0.38	53996	25.83	0.25	54000	24.88	0.12
54058	25.47	0.16	54000	25.95	0.31	54019	26.14	0.57
. . .	. . .	. . .	54019	25.05	0.16	54023	24.66	0.14
. . .	. . .	. . .	54023	25.56	0.24	54035	25.91	0.51
. . .	. . .	. . .	54031	26.12	0.54	54053	24.68	0.22
. . .	. . .	. . .	54035	25.67	0.26	54058	25.99	0.47
. . .	. . .	. . .	54053	26.48	0.68	. . .	. . .	. . .
. . .	. . .	. . .	54058	27.51	1.00	. . .	. . .	. . .

Table F.1: SN2213-1745 *g'r'i'* magnitudes for 2005 and 2006

day (MJD)	g'	error	day (MJD)	r'	error	day (MJD)	i'	error
54090	26.48	0.30	54062	25.78	0.28	54061	25.71	0.30
54096	26.10	0.24	54067	26.34	0.42	54083	26.47	0.61
54117	26.41	0.27	54083	26.36	0.56	54090	25.56	0.19
54121	26.57	0.33	54113	25.85	0.40	54095	25.85	0.33
54124	26.46	0.33	54117	25.88	0.23	54113	25.56	0.36
54179	26.44	0.29	54122	25.98	0.26	54117	25.62	0.27
54197	26.31	0.33	54172	25.92	0.61	54120	26.05	0.31
54202	25.61	0.18	54176	26.00	0.47	54123	26.20	0.62
54229	26.24	0.33	54183	25.85	0.31	54126	26.10	0.60
54234	25.97	0.24	54186	25.95	0.45	54140	25.99	0.42
54237	26.05	0.23	54197	26.12	0.43	54144	26.16	0.45
54420	25.79	0.18	54201	25.45	0.23	54172	25.46	0.24
54446	25.94	0.33	54205	25.86	0.26	54176	25.98	0.59
54452	26.18	0.28	54209	25.85	0.26	54179	25.98	0.43
54469	26.41	0.28	54213	25.96	0.37	54183	25.38	0.29
54472	25.92	0.17	54229	25.80	0.27	54186	26.02	0.59
54476	26.25	0.22	54234	25.48	0.25	54197	26.26	0.40
54479	26.22	0.19	54237	25.30	0.17	54201	25.07	0.26
54508	26.10	0.19	54418	24.84	0.19	54205	25.49	0.21
54510	25.69	0.23	54420	25.12	0.19	54209	25.22	0.24
54524	26.38	0.23	54445	24.78	0.17	54213	25.38	0.21
54528	26.35	0.23	54452	25.09	0.22	54229	25.15	0.18
54531	26.31	0.22	54469	25.15	0.13	54234	24.91	0.21
54535	26.16	0.21	54472	25.16	0.13	54237	25.09	0.15
54556	26.55	0.43	54476	25.34	0.16	54418	24.66	0.16
54558	26.11	0.19	54479	25.24	0.14	54420	24.38	0.16
54587	26.54	0.40	54481	24.81	0.17	54448	24.95	0.29
54591	26.27	0.23	54507	25.56	0.39	54452	24.87	0.20
54615	26.01	0.21	54508	25.50	0.19	54468	24.68	0.10
. . .	. . .	. . .	54510	25.39	0.25	54472	24.42	0.15
. . .	. . .	. . .	54512	25.41	0.37	54475	24.57	0.11
. . .	. . .	. . .	54524	25.49	0.21	54479	24.85	0.15
. . .	. . .	. . .	54528	25.44	0.19	54481	24.86	0.22
. . .	. . .	. . .	54531	25.23	0.15	54507	26.08	0.88
. . .	. . .	. . .	54535	25.45	0.20	54507	25.44	0.34
. . .	. . .	. . .	54538	25.56	0.27	54510	24.69	0.23
. . .	. . .	. . .	54554	25.73	0.32	54512	24.37	0.16
. . .	. . .	. . .	54555	25.74	0.34	54524	24.88	0.20
. . .	. . .	. . .	54556	25.29	0.19	54528	24.85	0.20
. . .	. . .	. . .	54558	25.45	0.19	54531	24.91	0.17
. . .	. . .	. . .	54562	25.90	0.33	54535	24.98	0.25
. . .	. . .	. . .	54587	25.58	0.37	54538	24.94	0.21
. . .	. . .	. . .	54591	25.17	0.15	54554	24.89	0.15
. . .	. . .	. . .	54594	25.34	0.20	54558	24.72	0.19
. . .	. . .	. . .	54597	25.97	0.59	54562	24.89	0.18
. . .	. . .	. . .	54615	25.13	0.20	54568	25.93	0.65
. . .	. . .	. . .	54619	25.34	0.37	54570	25.26	0.39
. . .	. . .	. . .	. . .	. . .	. . .	54587	24.75	0.23
. . .	. . .	. . .	. . .	. . .	. . .	54591	24.65	0.19
. . .	. . .	. . .	. . .	. . .	. . .	54594	24.75	0.19
. . .	. . .	. . .	. . .	. . .	. . .	54597	24.74	0.27
. . .	. . .	. . .	. . .	. . .	. . .	54614	24.56	0.13
. . .	. . .	. . .	. . .	. . .	. . .	54618	24.90	0.27

Table F.2: SN1000+0216 $g'r'i'$ magnitudes for 2006 and 2007

REFERENCES *(continued)*

30. Oke, J. B. *et al.* The Keck Low-Resolution Imaging Spectrometer *Publ. Astron. Soc. Pacif.* **107**, 375–385 (1995)

31. Gardner, J. P., Brown, T. M. & Ferguson, H. C. Ultraviolet Galaxy Counts from Space Telescope Imaging Spectrograph Observations of the Hubble Deep Fields *Astrophys. J. Lett.* **542**, 79–82 (2000)

32. Ferguson, H. C. *et al.* The Size Evolution of High-Redshift Galaxies *Astrophys. J. Lett.* **600**, 107–110 (2004)

33. Drake, A. J. *et al.* The Discovery and Nature of Optical Transient CSS100217: 102913+404220 *Astrophys. J.* **735**, 106 (2011)

34. Dahlén, T. & Fransson, C. Rates and redshift distributions of high-z supernovae *Astron. Astrophys.* **350**, 349–367 (1999)

35. Botticella, M. T. *et al.* Supernova rates from the Southern inTermediate Redshift ESO Supernova Search (STRESS) *Astron. Astrophys.* **279**, 49–66 (2008)

36. Madau, P., Pozzetti, L. & Dickinson, M. The Star Formation History of Field Galaxies *Astrophys. J.* **498**, 106–116 (1998)

37. Hopkins, A. M. & Beacom, J. F. On the Normalization of the Cosmic Star Formation History *Astrophys. J.* **651**, 142–154 (2006)

38. Guy, J. *et al.* The Supernova Legacy Survey 3-year sample: Type Ia supernovae photo-metric distances and cosmological constraints *Astron. Astrophys.* **523**, A7 (2010)

39. Regnault, N. *et al.* Photometric calibration of the Supernova Legacy Survey fields *Astron. Astrophys.* **506**, 999–1042 (2009)

40. Woosley, S. E., Blinnikov, S. & Heger, A. Pulsational pair instability as an explanation for the most luminous supernovae *Nature* **450**, 390–392 (2007)

41. Kennicutt, R. C. Star Formation in Galaxies Along the Hubble Sequence *Ann. Rev. Astron. Astrophys.* **36**, 189–232 (1998)

42. Larson, R. B. & Tinney, B. M. Star formation rates in normal and peculiar galaxies *Astrophys. J.* **219**, 46–59 (1978)

43. Barton, E. J., Geller, M. J. & Kenyon, S. J. Tidally Triggered Star Formation in Close Pairs of Galaxies *Astrophys. J.* **520**, 660–679 (2000)

44. Barton Gillespie, E. J., Geller, M. J. & Kenyon, S. J. Tidally Triggered Star Formation in Close Pairs of Galaxies II. Constraints on Burst Strengths and Ages *Astrophys. J.* **582**, 668–688 (2003)

45. Overzier, R. *et al.* Hubble Space Telescope Morphologies of Local Lyman Break Galaxy Analogs. I. Evidence for Starbursts Triggered by Merging *Astrophys. J.* **677**, 37–62 (2008)

46. Overzier, R. *et al.* Morphologies of Local Lyman Break Galaxy Analogs. II. A Compari-son with Galaxies at z 2-4 in ACS and WFC3 Images of the Hubble Ultra Deep Field *Astrophys. J.* **710**, 979–991 (2010)

47. Mannucci, F. *et al.* LSD: Lyman-break galaxies Stellar populations and Dynamics - I. Mass, metallicity and gas at z $\sim$ 3.1 *Mon. Not. R. Astron. Soc.* **398**, 1915–1931 (2009)

48. Neill, J. D. *et al.* The Extreme Hosts of Extreme Supernova *Astrophys. J.* **727**, 15 (2011)

49. Pan, T., Loeb, A. & Kasen, D. Pair-instability supernovae via collision runaway in young dense star clusters *Mon. Not. R. Astron. Soc.* **423**, 2203-2208 (2012)

50. Fransson, C. *et al.* Optical and Ultraviolet Spectroscopy of SN 1995N: Evidence for Strong Circumstellar Interaction *Astrophys. J.* **572**, 350–370 (2002)

51. Fransson, C. *et al.* Hubble Space Telescope and Ground-Based Observations of SN 1993J and SN 1998S: CNO Processing in the Progenitors *Astrophys. J.* **622**, 991–1007 (2005)

52. Shapley, A. E. *et al.* Rest-Frame Ultraviolet Spectra of z$\sim$3 Lyman Break Galaxies *Astrophys. J.* **588**, 65–89 (2003)